High-pressure Structural Studies and Pressure-induced Sensitization of 3,4,5-trinitro-1*H*-pyrazole

Nurunnisa Atceken,[a,b] Jack Hemingway,[b] Craig L. Bull,[b,c] Xiaojiao Liu,[b] Adam A. L. Michalchuk,[d] Sumit Konar,[b.e] Carole A. Morrison,[b]* and Colin R. Pulham[b]*

[a]Department of Materials Science and Engineering, İzmir Institute of Technology, Urla, 35430, İzmir, Turkey.

[b]EaStCHEM School of Chemistry and Centre for Science at Extreme Conditions, The University of Edinburgh, King's Buildings, David Brewster Road, Edinburgh EH9 3FJ, U.K.

[c]ISIS Neutron and Muon Facility, STFC Rutherford Appleton Laboratory, Harwell, Oxford, Didcot, Oxfordshire OX11 0QX, U.K.

[d] School of Chemistry, University of Birmingham, Edgebaston, Birmingham, B15 2TT, UK

[e]Joseph Banks Laboratories, School of Chemistry, University of Lincoln, Lincoln, U.K.

E-mail: c.r.pulham@ed.ac.uk

E-mail: c.morrison@ed.ac.uk

Supporting Information

Part I: Neutron powder diffraction data

Part 2: Single-Crystal X-ray diffraction data

Part 3: Computational modelling

Part 1: Neutron powder diffraction data

Table S1. Variation in the unit-cell parameters of 3,4,5-TNP (Form I) with pressure, derived from neutron powder diffraction experiments.

| Pressure (GPa)	a (Å)	b (Å)	c (Å)	° (deg)	V (Å^3)	wR	GOF
0.08(3)	15.1685(14)	8.2791(8)	17.1995(20)	92.258(10)	2158.3(3)	4.65%	1.85
0.24(4)	15.1096(14)	8.2388(8)	17.1381(20)	92.240(10)	2131.8(3)	4.89%	1.37
0.56(4)	15.0127(14)	8.1765(8)	17.0501(19)	92.217(11)	2091.4(2)	4.86%	1.34
0.94(3)	14.8868(12)	8.1009(6)	16.9416(16)	92.137(9)	2041.7(2)	4.24%	1.63
1.17(4)	14.8192(13)	8.0595(7)	16.8916(17)	92.106(10)	2016.1(2)	4.64%	1.25
1.31(4)	14.7831(13)	8.0363(7)	16.8668(17)	92.091(10)	2002.5(2)	4.70%	1.26
1.48(4)	14.7374(12)	8.0076(6)	16.8368(15)	92.073(10)	1985.6(2)	4.15%	2.07
1.59(4)	14.6997(13)	7.9827(7)	16.8119(17)	92.063(11)	1971.5(2)	4.83%	1.28
1.81(4)	14.6509(13)	7.9565(7)	16.7874(17)	92.006(11)	1955.7(2)	4.72%	1.24
1.99(4)	14.6027(13)	7.9293(6)	16.7675(17)	91.972(10)	1940.4(2)	4.27%	1.57
2.12(4)	14.5646(14)	7.9067(7)	16.7509(18)	91.944(11)	1927.9(2)	4.63%	1.20
2.31(4)	14.5338(15)	7.8820(7)	16.7371(20)	91.969(12)	1916.2(2)	4.64%	1.25
2.53(4)	14.5072(15)	7.8613(7)	16.7238(21)	91.984(12)	1906.1(2)	4.72%	1.21
2.68(4)	14.4765(13)	7.8391(6)	16.7086(20)	91.996(11)	1895.0(2)	4.25%	1.86
2.85(4)	14.4512(15)	7.8200(7)	16.6974(22)	92.009(13)	1885.8(2)	4.69%	1.18
3.02(4)	14.4205(14)	7.7985(7)	16.6817(21)	92.016(12)	1874.8(2)	4.68%	1.17
3.23(4)	14.3879(13)	7.7744(6)	16.6731(20)	92.022(11)	1863.9(2)	4.25%	1.49
3.34(5)	14.3636(13)	7.7548(7)	16.6619(21)	92.031(12)	1854.8(2)	4.62%	1.13
3.58(5)	14.3312(13)	7.7337(7)	16.6455(21)	92.024(11)	1843.7(2)	4.60%	1.12
3.77(5)	14.3001(13)	7.7112(7)	16.6294(21)	92.022(12)	1832.6(2)	4.69%	1.13
4.02(5)	14.2726(13)	7.6828(7)	16.6126(21)	92.110(12)	1820.4(2)	4.58%	1.32
4.37(7)	14.2292(16)	7.6577(9)	16.5867(26)	92.073(14)	1806.2(3)	5.59%	0.91
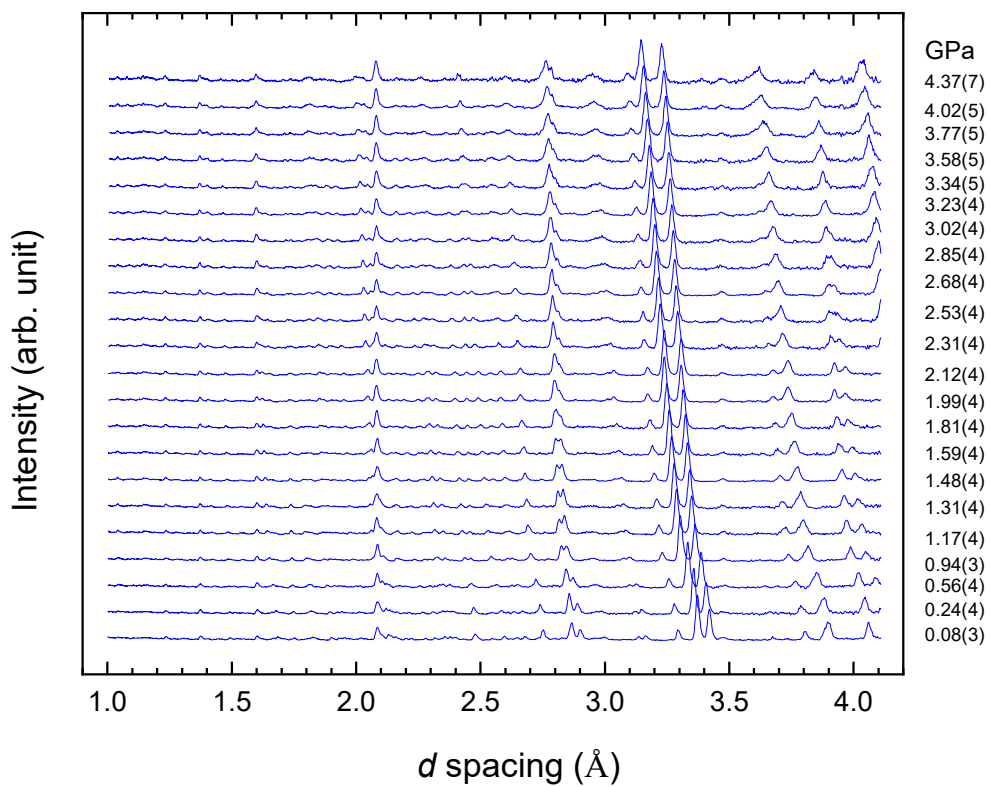
Figure S1 Sequence of neutron powder diffraction patterns obtained for 3,4,5-TNP upon increasing pressure.

Figure S2 Ruptured Ti-Zr gasket and cracked anvil after violent decomposition at 4.46 GPa.

Figure S3 Rietveld refinement plots of neutron powder diffraction patterns of 3,4,5-TNP at elevated pressures. Experimental (observed) data are shown as red dots, the solid black line shows the calculated profile from Rietveld refinement; the bottom blue trace shows the residual intensity I(obs)−I(calc). The positions of Bragg peaks for each phase are shown as vertical tick marks: from top to bottom Al_2O_3, Pb, TNP, and ZrO_2
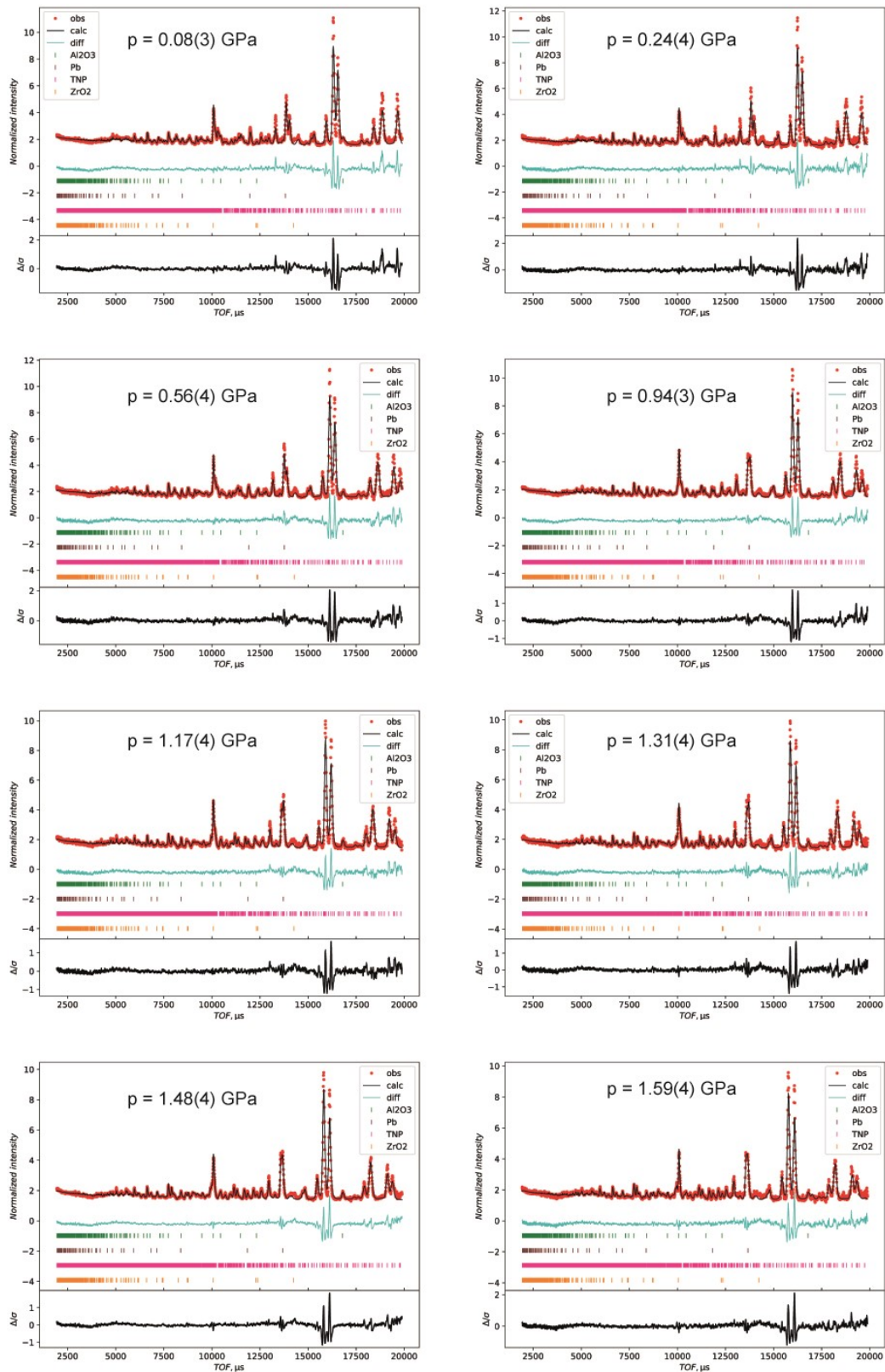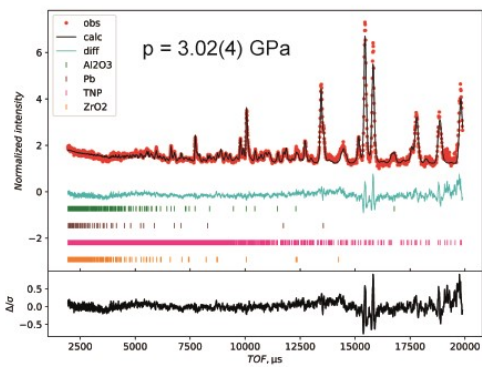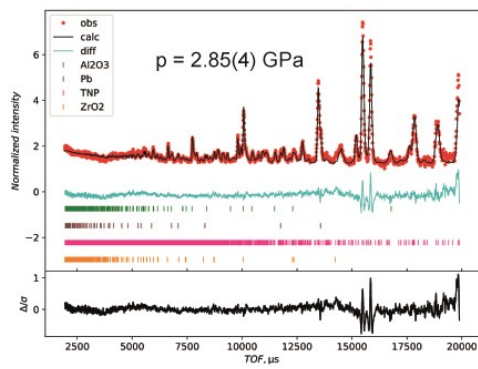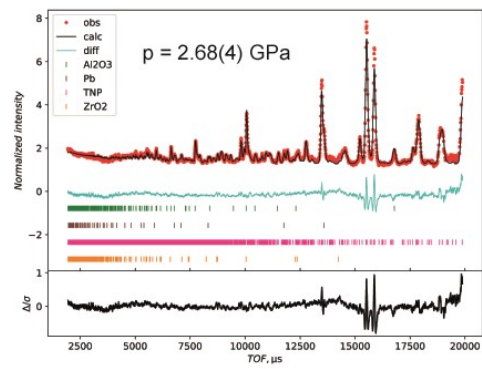
Figure S3 (Continued)
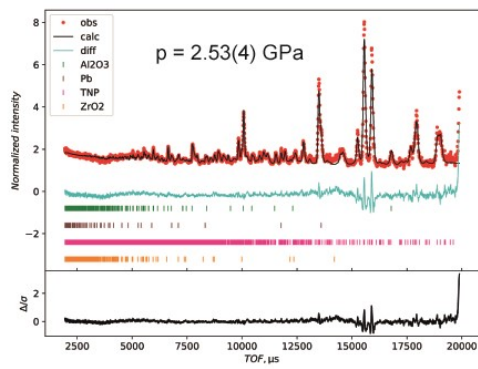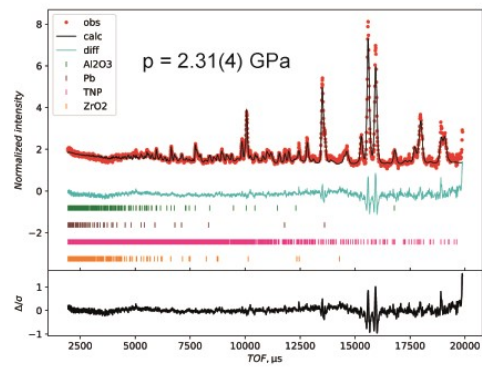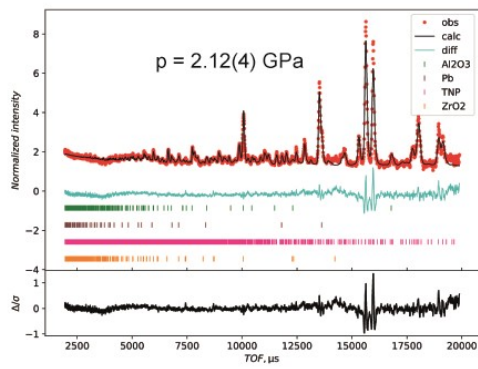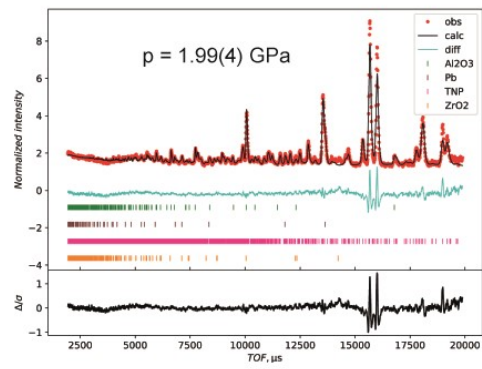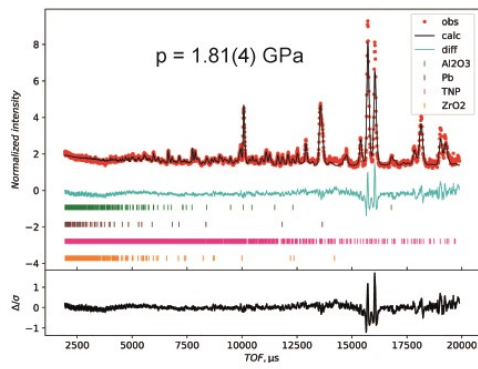
Figure S3 (Continued)
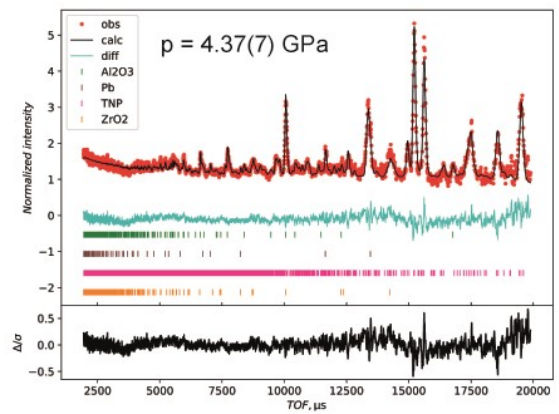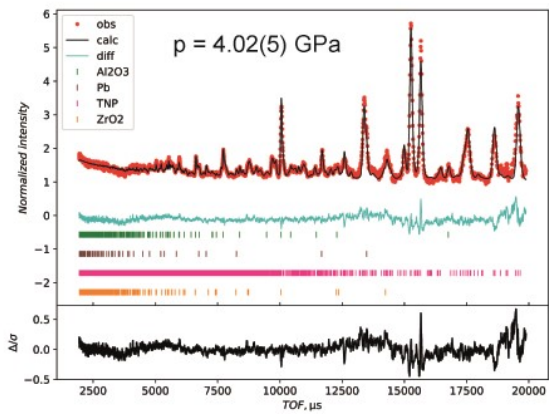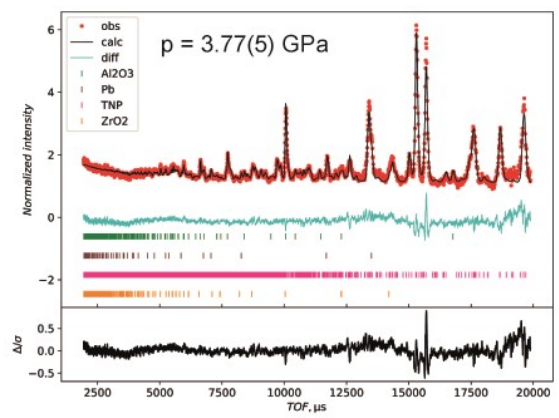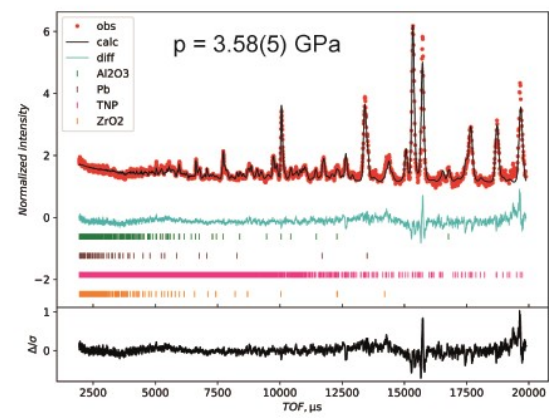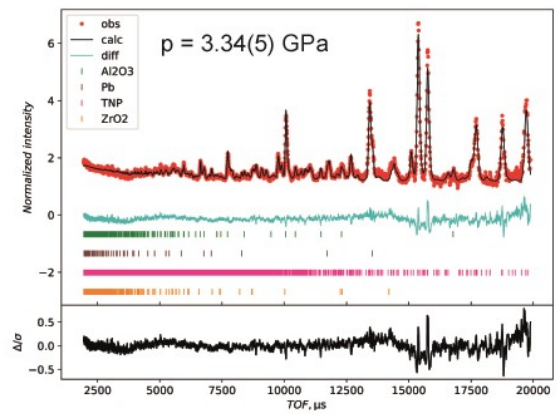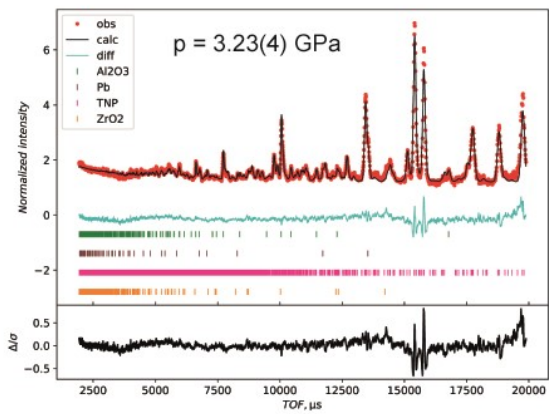
Figure S4 Compressibility indicatrix for 3,4,5-TNP showing orientation of the principal axes of
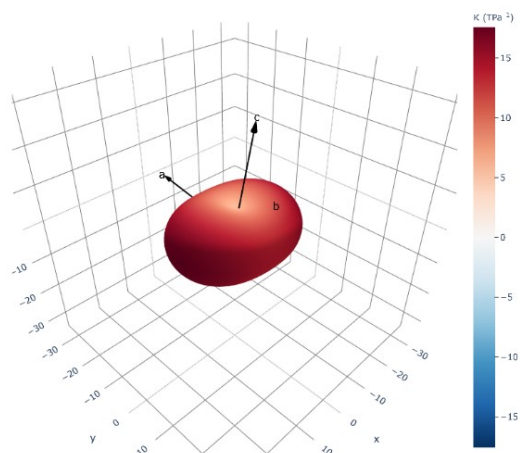
compressibility with respect to the crystallographic axes

Figure S5 Overlays of the three independent TNP molecules in the asymmetric unit based on structures obtained from Rietveld refinements of neutron powder diffraction data over the pressure range 0.08–4.37 GPa

Part 2: Single-Crystal X-ray diffraction data

Table S2 Unit-cell parameters obtained from high-pressure single-crystal X-ray diffraction experiments

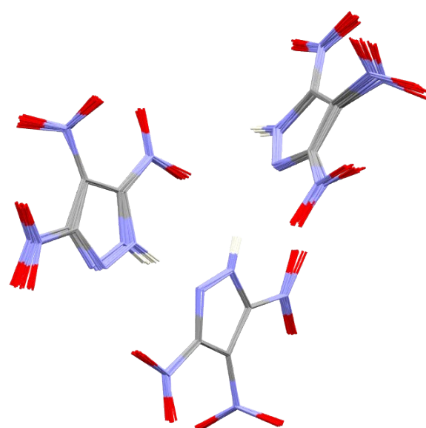| GPa	Volume	a (Å)	b (Å)	c (Å)	β-angle(°)
0.20	2133.3(3)	15.104(1)	8.246(1)	17.141(1)	92.235(4)
0.58	2062.7(4)	14.937(2)	8.1341(1)	16.989(2)	92.17(7)
1.11	2003.1(3)	14.7836(11)	8.0383(8)	16.8670(12)	92.078(4)
1.71	1955.3(2)	14.645(1)	7.9546(7)	16.7946(9)	92.018(4)
2.60	1887.3(2)	14.453(1)	7.8178(8)	16.713(1)	92.015(4)
3.81	1812.2(2)	14.2569(7)	7.6573(6)	16.6118(8)	92.197(3)
5.30	1742.3(3)	19.571(1)	7.6509(8)	14.6982(9)	127.661(2)
6.59	1695.3(3)	19.399(1)	7.5957(8)	14.529(2)	127.637(3)
7.30	1674.0(5)	19.319(2)	7.567(1)	14.458(3)	127.623(5)

Figure S6 Definition and variation of torsion angles ($\tau1-\tau9$) with increasing pressure; parameters obtained from crystal structures obtained from high-pressure single crystal X-ray diffraction experiments.
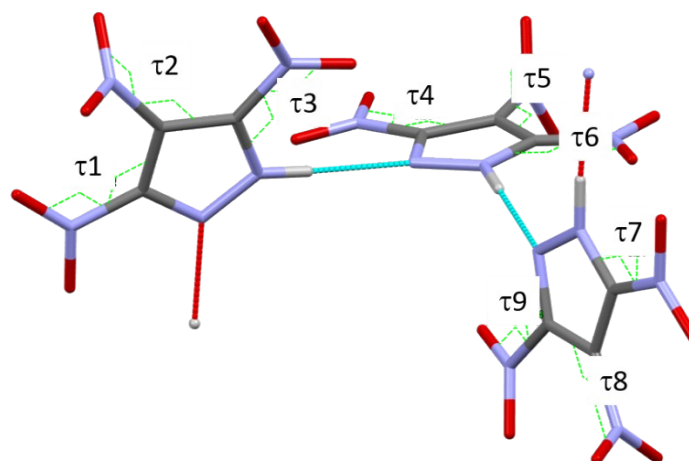
GPa	$\tau1$	$\tau2$	$\tau3$	$\tau4$	$\tau5$	$\tau6$	$\tau7$	$\tau8$	$\tau9$
Form I									
0.20	10.2	68.6	5.8	-0.6	-98.0	-2.2	6.2	-113.5	14.0
0.58	10.0	69.6	7.7	-1.4	-97.4	-1.6	6.8	-115.6	14.5
1.10	11.1	69.0	8.9	-0.9	-95.2	-2.5	8.0	-116.4	16.7
1.71	11.7	68.2	8.9	-1.3	-94.6	-3.4	7.5	-115.9	16.7
2.60	11.5	70.3	8.2	-1.6	-92.7	-4.7	6.8	-117.4	17.9
3.80	13.2	69.8	9.4	-2.8	-90.7	-6.6	6.1	-118.0	21.9
Form II									
5.3	-4.1	77.4	-4.9	11.5	-123.9	4.1	-2.4	-113.6	6.8
6.6	-0.3	64.1	6.7	1.9	-120.3	7.8	-6.1	-105.9	-3.7
7.3	0.8	64.4	4.8	0.8	-120.8	8.0	-4.5	-106.0	-2.2
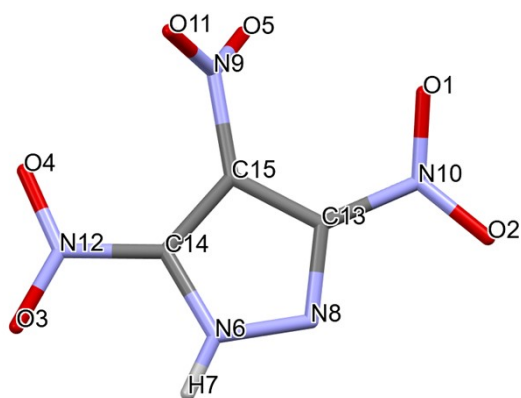
	Form I	Form II
O1	4.091	4.088
O2	4.089	4.091
O3	4.088	4.091
O4	4.087	4.081
O5	4.084	4.083
N6	3.480	3.480
H7	0.423	0.424
N8	3.535	3.533
N9	3.372	3.374
N10	3.373	3.371
O11	4.085	4.089
N12	3.371	3.371
C13	2.968	2.968
C14	2.963	2.962
C15	2.991	2.990

Table S3: Calculated Hirshfeld charge populations (B3LYP/6-311G* using Gaussian16)[S1] for molecule 1 in Form I (0.2 GPa structure) and Form II (5.3 GPa structure), based on single point energy calculations of the experimental crystal geometries. Note for the Form II geometry, H7 was manually added using the same structural features (bond length, angle and torsional angle to the ring) as defined by the Form I structure.

High similarities in charge distributions indicate similar molecular properties in the two phases. This indicates that sensitivity prediction models based on molecular parameters such as charge distributions and bond energies[S2-S6] are insufficient to capture the different initiation behaviors of Forms I and II.

Part 3: Computational modelling

Geometry optimisation

Table S4 Experimental and calculated unit cell parameters for Form I and Form II of 3,4,5-TNP

Polymorph		a/Å	b/Å	c/Å	β/°	V/Å³	ΔV/Å³
Form I	Exp	15.1586(13)	8.2781(8)	17.2014(16)	92.275(2)	2156.81	
	Calc	15.4863	8.3610	17.3980	92.222	2252.48	+4.4%
Form I	Calc*	14.3040	7.7678	16.3512	91.689	1816.00	-15.8%
Form II	Exp	19.5713(11)	7.6509(8)	14.6982(9)	127.661(2)	1742.30	
	Calc*	19.6649	7.7154	14.8667	127.845	1781.21	+2.2%

*Optimised in the presence of 5.3 GPa external pressure.

Table S5 Variation in calculated torsion angles ($\tau1-\tau9$) for Form I and Form II of 3,4,5-TNP

Pressure (GPa)	$\tau1$	$\tau2$	$\tau3$	$\tau4$	$\tau5$	$\tau6$	$\tau7$	$\tau8$	$\tau9$
Form I	10.0	72.9	7.2	1.0	-95.5	-1.1	7.4	-110.9	13.9
Form II*	-1.9	74.3	-3.4	8.4	-119.0	4.7	-1.9	-113.9	5.6

*Optimised in the presence of 5.3 GPa external pressure.

Impact sensitivity prediction modelling

To predict the impact sensitivity for a molecular energetic compound using the vibrational up-pumping method, a number of parameters must first be defined. Firstly, the position of Ω_{max}, denoting the top of the phonon bath is determined by calculating the centre of mass displacements from the simulated eigenvectors, and noting where the switch-over from large displacements (*i.e.* lattice mode behaviour, denoted as q) to negligible displacements (*i.e.* molecular mode behaviour, denoted as Q) occurred. This allows the number of phonon bath modes to be defined. Secondly, the degree of lattice mode heating arising due to the adsorption of the shock wave energy, i.e. T_{shock}, is estimated as a ratio of the predicted bulk heat capacity (C_{tot}) to the phonon (C_{ph}) . With these parameters thus set, the vibrational up-pumping method then explores three mode scattering pathways to generate the two phonon density of states ($\Omega^{(2)}$) envelope: (i) $q_1 + q_1$ (*i.e.* a phonon bath mode (q) scattering with itself, to create a new state, akin to the first overtone state), (ii) $q_1 + q_2$ (*i.e.* two separate phonon bath modes combining to create a new state, akin to a combination mode). The maximum wavenumber that can be reached by these processes is $2\Omega_{max}$. Modes that appear in this region are termed doorway modes, Q_D. These contribute to the final scattering pathway, which is (iii) $q + Q_D$; this creates new states that fall in the 2-3 Ω_{max} range of $\Omega^{(2)}$. The overlap between the projected $\Omega^{(2)}$ onto the underlying density of states plot in the 1-3 Ω_{max} up-pumping window provides a quantitative measure of the ability of the molecular crystal vibrations to trap the shock wave energy in the molecular modes, which we take in this work as the metric for simulated impact sensitivity.

As the two forms of TNP contain different numbers of molecules, *Z*, in their respective ***primitive*** unit cells, the up-pumping process must be normalised, on a per-phonon mode, per-molecule basis. To achieve this, the initial density of states plot is normalised with respect to the number of phonon

modes prior to the up-pumping process; following up-pumping the integration of $\Omega^{(2)}$ onto the phonon density of states in the up-pumping window is then divided by Z.

Obtaining Ω_{max} for Form I and Form II TNP

The centre of mass (CoM) displacement plots shown in Figure S7 indicate a switch over in eigenvector behavior from lattice mode (large CoM change) to molecular mode behaviour (small CoM change) at 214 cm^{-1} and 256 cm^{-1} for Form I and Form II, respectively. Re-optimizing Form I in the presence of a 5.3 GPa external pressure raises Ω_{max} to 252 cm^{-1}.
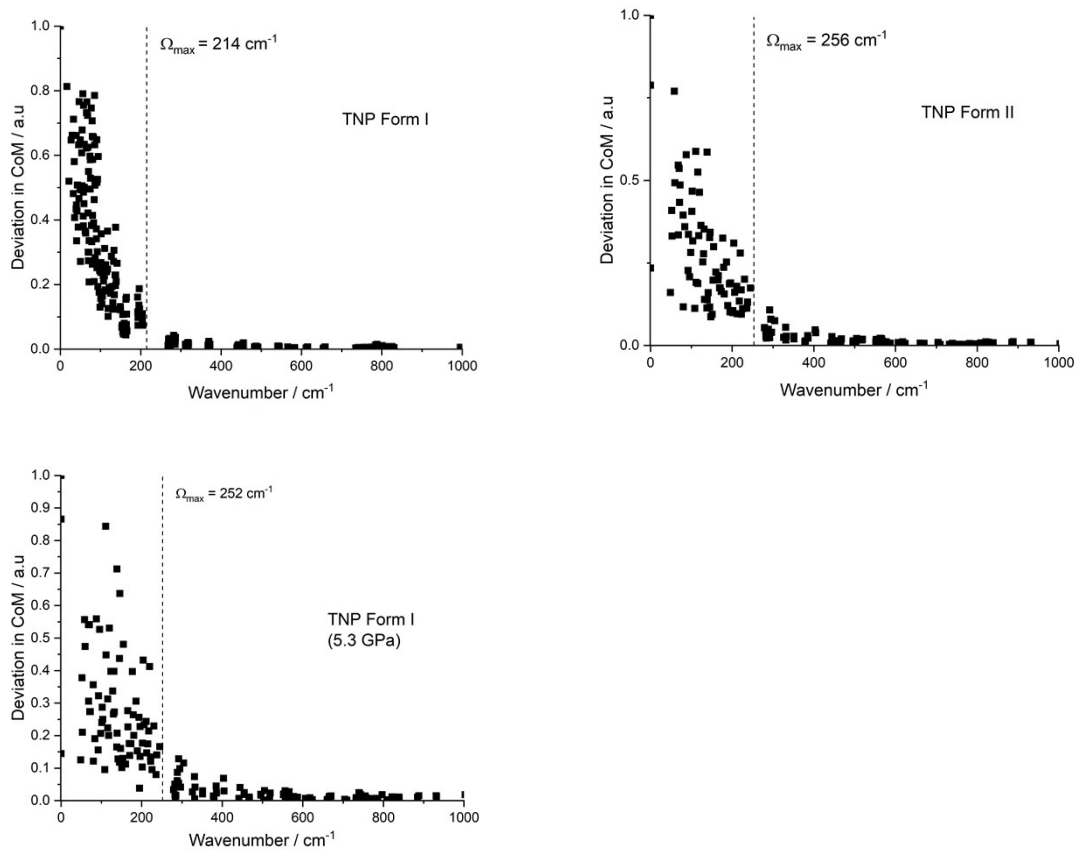

Figure S7 Centre of Mass displacement vs. wavenumber plots for Form I and Form II and compressed Form I, with a yellow region indicating the location in which Ω_{max} can be found.

Obtaining T_{shock} for Form I, Form II, and compressed Form I

The rate of phonon mode heating is estimated by obtaining the ratio of the bulk heat capacity (C_{tot}) to the phonon heat capacity (C_{ph}), assuming

$$C_v = \int \frac{\partial n}{\partial T} \hbar \omega g(\omega).d\omega$$

Equation S1

where n is phonon population, T is temperature (K), ω is frequency, $g(\omega)$ is the density of states and $\hbar$ is the Planck constant divided by 2π. The resulting cumulative heat capacities for Forms I and II are shown in Figure S8. This process permits the contribution of the low-energy phonon modes to the bulk

heat capacity to be obtained; this distinction is important as the low-energy phonon modes have a correspondingly lower heat capacity and subsequently superheat following mechanical impact. The ratio of the bulk heat capacity (C_{tot}) to the phonon (C_{ph}) yields a scaling factor, from which a representative value for T_{shock} is obtained; this is summarised in Table S6.
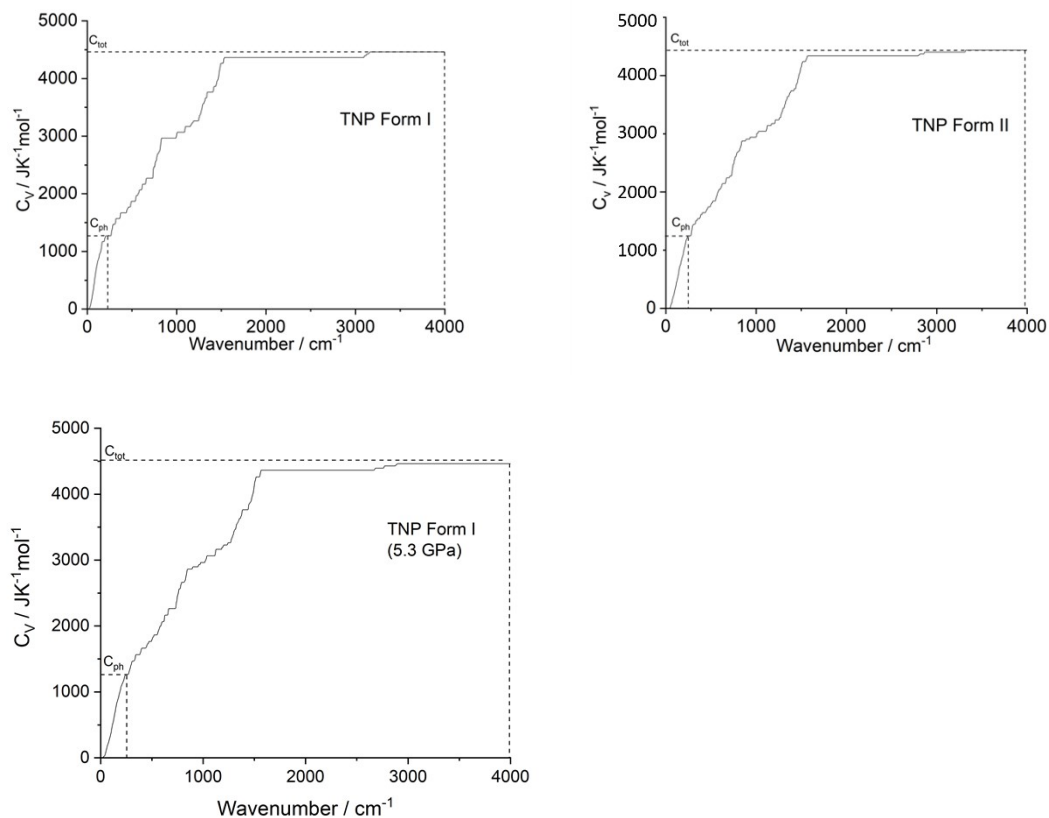

Figure S8 Cumulative vibrational heat capacity, as expressed by Equation 1 for Forms I, II and compressed Form I of 3,4,5-TNP

Table S6 Ratios of predicted total (C_{tot}) and phonon-bath only (C_{ph}) heat capacities and the resulting phonon-bath shock temperatures (T_{shock}) used in the impact-sensitivity prediction model for TNP. Note a value of C_{tot}/C_{ph} = 5.00 equates to T_{shock} = 3278 K, from our earlier work, see references in main text).

	Form I	Form II	Form I (5.3 GPa)
C_{tot}/J K^{-1} mol^{-1}	4463	4438	4463
C_{ph}/J K^{-1} mol^{-1}	1278	1246	1266
C_{tot} / C_{ph}	3.49	3.56	3.53
T_{shock}/K	2288	2334	2314

Finally, the parameters used to generate $\Omega^{(2)}$, and the subsequent projection onto g(ω) to yield the up-pumped densities for the three optimised structures of 3,4,5-TNP are summarised in Table S7.

Table S7 Parameters used to calculate the relative up-pumped densities of polymorphs of TNP. Z denotes the number of molecules in the each *primitive* unit cell, Y is the number of amalgamated vibrations per molecule, and T_{shock} is the temperature adopted for the phonon bath modes.

Polymorph	Ω_{max}	Z	$Z(6+Y)$	Y	T_{shock}/K	Up-pumped density/a.u.
Form I	214	12	156	7	2288	31931
Form II	256	6	78	7	2334	86448
Form I (5.3 GPa)	252	12	156	7	2314	88674

References

S1   Gaussian 16, Revision A.03, M. J. Frisch, G. W. Trucks, H. B. Schlegel, G. E. Scuseria, M. A. Robb, J. R. Cheeseman, G. Scalmani, V. Barone, G. A. Petersson, H. Nakatsuji, X. Li, M. Caricato, A. V. Marenich, J. Bloino, B. G. Janesko, R. Gomperts, B. Mennucci, H. P. Hratchian, J. V. Ortiz, A. F. Izmaylov, J. L. Sonnenberg, D. Williams-Young, F. Ding, F. Lipparini, F. Egidi, J. Goings, B. Peng, A. Petrone, T. Henderson, D. Ranasinghe, V. G. Zakrzewski, J. Gao, N. Rega, G. Zheng, W. Liang, M. Hada, M. Ehara, K. Toyota, R. Fukuda, J. Hasegawa, M. Ishida, T. Nakajima, Y. Honda, O. Kitao, H. Nakai, T. Vreven, K. Throssell, J. A. Montgomery, Jr., J. E. Peralta, F. Ogliaro, M. J. Bearpark, J. J. Heyd, E. N. Brothers, K. N. Kudin, V. N. Staroverov, T. A. Keith, R. Kobayashi, J. Normand, K. Raghavachari, A. P. Rendell, J. C. Burant, S. S. Iyengar, J. Tomasi, M. Cossi, J. M. Millam, M. Klene, C. Adamo, R. Cammi, J. W. Ochterski, R. L. Martin, K. Morokuma, O. Farkas, J. B. Foresman, and D. J. Fox, Gaussian, Inc., Wallingford CT, 2016.

S2   Politzer, P.; Murray, J. S. Some molecular/crystalline factors that affect the sensitivities of energetic materials: molecular surface electrostatic potentials, lattice free space and maximum heat of detonation per unit volume. *J. Mol. Model*. **2015**, *21*, 25.

S3   Aina, A. A.; Misquitta, A. J.; Phipps, M. J. S.; Price, S. L. Charge Distributions of Nitro Groups Within Organic Explosive Crystals: Effects on Sensitivity and Modeling. *ACS Omega* **2019**, *4*, 8614-8625.

S4   Jenson, T. L.; J. F. Moxnes, J. F.; Unneberg, E.; Christensen, D. J. Models for predicting impact sensitivity of energetic materials based on the trigger linkage hypothesis and Arrhenius kinetics. *Mol. Model*. **2020**, *26*, 65.

S5   Cawkwell, M. J.; Davis, J.; Lease, N; Marrs, F . W.; Burch, A.; Ferreira, S.; Manner, V. W. Understanding Explosive Sensitivity with Effective Trigger Linkage Kinetics. *ACS Phys. Chem. Au* **2022**, *2*, 448-458.

S6   Mathieu, D. Sensitivity of Energetic Materials: Theoretical Relationships to Detonation Performance and Molecular Structure. *Ind. Eng. Chem. Res*. **2017**, *56*, 8191-8201.